A study on CO_2 decomposition to CO and O_2 by the combination of catalysis and dielectric barrier discharges at low temperatures and ambient pressure

Kui Zhang[1*], Guangru Zhang[1], Xiaoteng Liu[1], Anh Phan[1], Kun Luo[2]

[1] School of Chemical Engineering and Advanced Materials, Newcastle University, Newcastle upon Tyne, NE1 7RU, UK

[2] College of Materials Science and Engineering, Guilin University of Technology, Guilin, 541004, China

Abstract

CO_2 decomposition to CO and O_2 was investigated in a dielectric-barrier discharge (DBD) reactor packed with $BaTiO_3$ balls, glass beads with different sizes, and a mixture of a Ni/SiO_2 catalyst and $BaTiO_3$ balls at lower temperatures and ambient pressure. The property of packing beads and the reactor configuration affected the reaction significantly. The Ni/SiO_2 catalyst samples were characterized by SEM, XRD, BET and TEM. The combination of a DBD plasma and a Ni/SiO_2 catalyst can enhance CO_2 decomposition apparently and a reaction mechanism of the plasma assisted CO_2 dissociation over the catalyst was proposed. In comparison with the result packed with glass balls (3 mm), the combination of $BaTiO_3$ beads (3 mm) with a stainless steel mesh significantly enhanced the CO_2 conversion and energy efficiency by a factor of 14.8, and that with a Ni/SiO_2 catalyst by a factor of 11.5 in a DBD plasma at a specific input energy (SIE) of 55.2 kJ/L and low temperatures (<115 °C).

Key Words: CO_2 conversion, Ni/SiO_2 catalyst, $BaTiO_3$, dielectric barrier discharge

* Corresponding author: Tel: +44 191 222 5747.
E-mail: kui.zhang@newcastle.ac.uk; luokun998@googlemail.com

1. Introduction

Climate change due to man-made emissions of GHGs such as CO_2, CH_4, N_2O and others is one of the major challenges facing mankind. Combustion of fossil fuels (coal, natural gas, and oil) for energy and transportation, certain industrial processes and land use change are responsible for the steady CO_2 concentration increase in the atmosphere since the industrial revolution. CO_2 emission not only results in an increase in the global mean temperature, but also constitutes an extensive waste of a natural carbon source. Therefore, mitigation of CO_2 has attracted worldwide attention. [1-5] Carbon capture and storage (CCS) and carbon capture and utilization (CCU) can capture CO_2 from point source such as power plants and industrial processes. CCU converts the captured CO_2 to value-added products, which is different from CCS which transfers the captured CO_2 to a suitable site for long-term storage. [6] CO_2 can be considered as a recycled carbon source and C_1 building block for fuels and chemicals.

CO_2 conversion to value-added chemicals/fuels has been attracted much attention over the past decades. [4, 7-9] CO_2 is the end product of the complete oxidation of fossil fuels and organic compounds, and it is difficult to be activated due to its intrinsic inert nature. Therefore, the use of CO_2 as chemical feedstock is limited to a few industrial process such as the production of urea and its derivatives, salicylic acid and carbonates. [10]

The hydrogenation of CO_2 to fuels and chemicals such as methane, methanol, formic acid and their derivatives has been intensively studied.[10-12] In general, the production of hydrocarbons and chemicals from CO_2 requires substantial energy input, effective reaction conditions (such

as high reaction temperature and high pressure), more hydrogen consumption, and active catalysts because CO_2 is a highly stable molecule.

CO is more reactive than CO_2 and it is a common feedstock for chemical industry.[13] In addition to be used for fuel synthesis, CO has many applications in the production of chemicals such as organic acids, esters, alcohols and other chemicals. The selective conversion of CO_2 to CO is a promising route for clean energy and chemicals by using CO_2 as a carbon source. [9, 14, 15]

The hydrogenation of CO_2 (or the reverse water gas shift (RWGS) reaction) (equation 1) can be used for CO production over catalysts at high reaction temperatures (>600 ºC). [10, 11] Reaction parameters, catalyst properties and reactor configuration affected the reaction apparently.[16] In the reaction, an excess of hydrogen is necessary to prevent the coke formation on the catalyst. Therefore, a big concern of the RWGS reaction is the product selectivity, H_2 consumption, and catalyst stability under reaction conditions.

$$CO_2 + H_2 \longrightarrow CO + H_2O \qquad (1)$$

(ΔH_{298K} = 41.2 kJ/mol)

CO_2 reforming of methane (equation 2) is a well-studied reaction which is of both scientific and industrial importance. It converts greenhouse gases (CO_2/CH_4) into synthesis gas (CO + H_2) over catalysts at high reaction temperatures (800-1000 ºC). [17] Operating at high temperatures may result in high energy costs and high capital investment. A major drawback of the catalytic CO_2 reforming of CH_4 is the catalyst deactivation because of the sintering of active sites and carbon deposition at high reaction temperatures.[18]

$$CO_2 + CH_4 \longrightarrow 2H_2 + 2CO \qquad (2)$$

ΔH_{298K} = 247 kJ/mol

Direct CO_2 conversion to CO and O_2 (equation 3) is a thermodynamically unfavourable reaction. Thermodynamic analysis shows that apparent CO_2 decomposition to CO and O_2 is difficult at reaction temperatures lower than 2000ºC. On the other hand, chemical kinetic study demonstrated that the reverse reaction, the reaction between CO and O_2 for CO_2, become dominant at higher reaction temperatures. Therefore, the decomposition of CO_2 to CO and O_2 could be favoured at non-equilibrium reaction conditions.

$$CO_2 \longrightarrow 0.5O_2 + CO \qquad (3)$$

ΔH_{298K} = 283 kJ/mol

Dielectric-barrier discharge (DBD) is a kind of non-thermal plasma (NTP), which is an alternative to the conventional catalytic chemical process operating at high temperatures. In a DBD, although the average temperature of the energetic electrons is in a range of 10,000 - 100,000 K (average electron energy: 1 - 10 eV), the actual gas temperature remains near ambient temperature. [19-21] Active radicals and ionic and excited atomic and molecular species are generated through electron-impact ionization, dissociation and excitation of the source gases, which can initiate plasma assisted chemical reactions at low temperatures. NTP could convert CO_2 to CO (and O_2) directly without consuming H_2 or methane at low temperatures and atmospheric pressure by using the renewable energy resources/green energy such as hydropower, wind power, solar power and biomass. After reaction, CO can be separated from the gas mixture of CO and O_2. The produced CO can be used as a feedstock for various applications. Furthermore, synthesis gas (CO + H_2) can be produced by introducing H_2 to the CO gas stream. The integration of NTP assisted direct CO_2 conversion to CO or synthesis gas (CO + H_2) and the established chemical processing may provide an alternative for the production of fuels and value-added chemicals from CO_2.

CO_2 decomposition to CO and O_2 assisted by non-equilibrium plasmas has been investigated under a variety of NTP conditions. Microwave plasma has been applied for CO_2 decomposition at various pressure. [22-25] Vesel and co-workers [23] studied the dissociation of CO_2 in a microwave plasma at low pressure (<1.13 torr). No black carbon formed on the surface of the quartz tube even after prolonged plasma operation, indicating that the dissociation of CO can be neglected in microwave plasma. A study on the efficiency of CO_2

dissociation in argon in an atmospheric pressure microwave plasma demonstrated that the combination of a plasma and a Rh/TiO_2 catalyst located in the downstream of the discharge region causes a drop in CO_2 conversion due to the reverse reaction of CO_2 decomposition on the catalyst surface. [22] Spencer and co-workers [26] studied the efficiency of CO_2 decomposition in a radio-frequency (RF) plasma at low pressure (0.08-0.28 torr). Although the conversion of CO_2 to CO can reach about 90%, the maximum energy efficiency was about 3%. In a capillary plasma reactor at low pressure (3.33-120 torr), CO_2 decomposition is predominated by electron impact dissociation of CO_2 and gas phase reverse reactions. [27] In a coaxial DC corona discharge, the dissociation of CO_2 could produce O_3 and CO. The CO_2 conversion was lower in a positive polarity discharge than that in a negative one under the same reaction condition. [28] CO_2 decomposition has been explored in DBD plasmas at atmospheric pressure by different research groups.[29-34] Paulussen and co-workers investigated the influence of reaction parameters such as frequency, power, temperature and gas flow rate on CO_2 decomposition in a tubular DBD reactor with one stainless steel electrode exposed to the plasma. [29] A plasma chemistry model for CO_2 splitting proposed by Aerts and co-workers shows reasonable agreement with the experimental conversion and energy efficiency in a DBD plasma.[30] The influence of permittivity of barrier materials on CO_2 decomposition in a planar DBD reactor with one stainless steel plate electrode exposed to the plasma was explored by Li and co-workers. [32-34] It was found that the CO_2 conversion over $Ca_{0.8}Si_{0.3}TiO_3$ is much higher than that over Al_2O_3 and SiO_2 glass barriers due to the great differences in their permittivity. Mei and co-workers [35] studied the effect of packing materials ($BaTiO_3$ and glass balls: 1 mm in diameter) on CO_2 decomposition by exposing a stainless steel rod electrode to the plasma and demonstrated that adding $BaTiO_3$ balls into the reactor enhanced the average electric field and mean electron energy which contributed to an enhancement of CO_2 conversion. A study on the decomposition of CO_2 in a coaxial dielectric packed-bed

plasma reactor with two corundum barriers revealed that the permittivity and the morphology of packing pellets (0.42-0.84 mm) influenced the reaction obviously because they could affect the electron energy distribution in the plasma. [36] Furthermore, the CO_2 dissociation could be influenced by the acid-base properties of the packing materials.

The aforementioned studies have been focused on CO_2 decomposition assisted by various NTPs. Although some literature is available on CO_2 decomposition assisted by DBD plasma with packing materials with different permittivity and acidity, few studies have been carried out on the effect of property of packing materials with identical size by eliminating the influence of metal electrode and the shape of the packing materials. A detailed study on the effect of the size of packing materials with the same dielectric constant, the reactor configuration, and the combination of a supported metal catalyst and DBD plasma on CO_2 decomposition is not available.

The purpose of this study was to study the effect of the property of packing materials (with identical size), the size of the packing materials (with identical permittivity and chemical property) by eliminating the influence of metal electrode, the reactor configuration, the stainless steel mesh, and a Ni/SiO_2 catalyst on CO_2 decomposition promoted by DBD plasmas. The synergistic effect of a DBD plasma and a Ni/SiO_2 catalyst (or a stainless steel mesh) on CO_2 decomposition will be investigated for the first time. The present study reveals that the combination of DBD plasma and a catalyst can enhance CO_2 decomposition apparently under NTP conditions.

2. Experimental Section

2.1 Materials

Glass beads: Soda-lime glass beads (3 mm, 4 mm, and 5 mm in diameter, respectively) were purchased from Sigma-Aldrich Ltd, and used in the reaction without further treatment.

$BaTiO_3$ beads: $BaTiO_3$ beads (3 mm in diameter) were purchased from Catal Ltd. The density of the $BaTiO_3$ beads was 3.3 g/cm^3. The dielectric constant of these beads was about 1000.

Ni/SiO_2 catalyst: A Ni/SiO_2 catalyst with molar ratio of $[Ni]/[SiO_2]$ = 1/4 was prepared from a precursor solution of colloidal silica (30 wt. % suspension in water, Sigma Aldrich, UK) as silica precursor and $Ni(NO_3)_2 \cdot 6H_2O$ (Purity: 97%, Sigma Aldrich, UK) as catalyst precursor. The catalyst preparation procedure included the following steps: Step1: to obtain the precursor solution with desired Ni/SiO_2 (molar ratio) = 1/4, 56.1 g of $Ni(NO_3)_2 \cdot 6H_2O$ was dissolved in 150 g of the precursor solution of colloidal silica; Step 2: to convert the precursor solution to solid pellets, 10 ml of the precursor solution was placed in a 19 cm diameter watch glass and irradiated at 1 kW power input using an Ethos EZ Microwave Furnace (Milestone S. R. L., Italy) at a relatively low temperature (250 ^{0}C) for 4 minutes. Repeat the operation to convert all the precursor solution into solid pellets. The size of the solid pellets selected for further treatment was 2-3 mm; Step 3: to obtain a Ni/SiO_2 catalyst, the above solid pellets were calcined at 550 °C in air for 2 h, and then reduced in a hydrogen flow of 50 mL/min at 550 °C for 24 h. At last, the reduced Ni/SiO_2 catalyst was cool down to

room temperature in the hydrogen flow. The density of the catalyst was 0.2g/cm^3. The BET surface area of it was 181 m^2/ g. Chemical analysis revealed that the amount of Ni (wt. %) in the Ni/SiO_2 catalyst was 19.7%.

$Ni/SiO_2/BaTiO_3$ beads: $Ni/SiO_2/BaTiO_3$ beads was a physical mixture of 50 cm^3 of reduced Ni/SiO_2 catalyst (2-3 mm pellets, 10g) and 50 cm^3 of $BaTiO_3$ Beads (3 mm in diameter, 165g).

2.2 Catalyst characterization

The morphology of the Ni/SiO_2 catalyst samples was investigated by a scanning electron microscopy (SEM, JSM-5300LV, Japan). A Beckman Coulter SA3100 surface area analyser was used to measure the specific surface area of the catalyst samples. The X-ray Diffraction (XRD) pattern of the catalyst samples was recorded by a PANalytical X'PERT Pro Diffractometer using CuKα1 source (λ=1.540598Å). The scan range (2θ) was from 10 to 100°. The fine structure of the catalyst samples was analysed with a Philips CM100 Transmission Electron Microscope (TEM), and the images were collected using an AMT CCD camera.

2.3 Catalytic reactions

Fig. 1 depicts a schematic of the experimental setup (Fig. 1a) and the DBD reactor with different configurations (Fig 1b-1e). The coaxial DBD reactor consisted of two coaxial quartz

tubes one inside the other. The outer tube had 32 mm inner diameter (ID) and 300 mm in length. The inner tube had 17 mm outer diameter (OD). The thickness of the two quartz tubes was 1.5 mm. Hence the gap between the two tubes was 7.5 mm. The length of the two stainless steel mesh electrodes was 173 mm, respectively, which gave a plasma volume of 100 cm^3 in the reactor. The first stainless steel mesh electrode was fixed on the inner surface of the inner tube, and the second one was either fixed on the external surface or on the internal surface of the external tube. The two electrodes were insulated to the plasma activated species when the second electrode was fixed on the external surface of the external tube (as shown in Fig. 1b). The second electrode was exposed to the plasma activated species when it was fixed on the internal surface of the external tube (as shown in Fig. 1c). To study the influence of a stainless steel mesh on the reaction, an extra stainless steel mesh was fixed on the inner surface of the external tube of the plasma reactor (as shown in Fig. 1d).

The discharge volume of the reactor was filled with 100 cm^3 of glass balls (3 mm, 4 mm, 5 mm in diameter, respectively), or 100 cm^3 of $BaTiO_3$ balls (3 mm in diameter), or the mixture of $BaTiO_3$ balls (3 mm in diameter) with the Ni/SiO_2 catalyst. Fig. 1e shows a picture of the reactor (as shown in Fig. 1b) packed with glass beads (3 mm in diameter). An alternating sinusoidal high voltage of up to 20 kV amplitude (peak-to-peak) with a frequency of about 25 kHz was applied to the two stainless steel mesh electrodes.

The plasma power source unit which could feed 0 - 150 W to the plasma reactor by adjusting the amplitude of the applied voltage was designed and manufactured by GAP Ltd. The power factor of the power source unit was higher than 0.95. The plasma power dissipated in the discharge was calculated by integrating the product of voltage and current. In addition, the

voltage-charge Lissajous diagrams were recorded by a TPS 2014 Four Channel Digital Storage Oscilloscope (Tektronix).

The wall temperature of the DBD reactor was measured by a thermocouple attached on the external surface of the reactor. To maintain the wall temperature of the plasma reactor, the plasma reactor was kept in a tubular furnace preselected at 100°C. The temperature of the furnace was controlled by a proportional with integral and derivative (PID) temperature controller.

CO_2 (BOC Industrial gases, UK) was introduced into the reactor from high pressure bottles via mass flow controllers (MFCs), admitting a total gas flow of 25 to 100 mL/min. the pressure in the reactor was monitored by a pressure gauge, and it could be adjusted by a back pressure valve at the exit of the DBD reactor.

An online Varian 450-GC equipped with a thermal conductivity detector (TCD) was used to analyse the reaction products (CO and O_2). The Varian 450-GC was connected to the outlet of the reactor by Teflon tubing. To monitor the change of volume flow as a consequence of chemical reactions, a constant flow of nitrogen (6.0 mL/min) (BOC Industrial gases, UK) as reference gas was added to the exit of the reactor (as shown in Fig. 1a). The results were reported in mole percent.

The CO_2 conversion is defined as

$$CO_2 \quad Conversion \quad (\%) = \frac{Moles\ of \quad CO_{2(in)} - Moles\ of \quad CO_{2(out)}}{Moles\ of \quad CO_{2(in)}} \times 100$$

The CO_2 conversion per unit energy (CO_2 CPUE) is defined as:

$$CO_2\ CPUE \quad (mmol/kJ) = \frac{mmol\ of \quad converted\ CO_2}{Energy\ consumed \quad (kJ)}$$

The specific input energy (SIE) is defined as

$$SIE \quad (kJ/l) = \frac{Plasma \quad power \quad (kW)}{CO_2 \quad flow\ rate \quad (l/s)}$$

The energy efficiency of a DBD plasma assisted CO_2 decomposition is defined as:

$$Energy \quad efficiency \quad (\%) = \frac{\Delta H_{298} \quad (kJ/mol)}{Energy \quad consumed \quad / mol\ of \quad converted \quad CO_2\,(kJ/mol)} \times 100$$

($CO_2 = CO + 0.5\ O_2$, $\Delta H_{298} = 283$ kJ/mol)

3. Results and discussion

3.1 Influence of packing materials

For a better understanding of the influence of the property of packing materials on CO_2 dissociation, the contribution of metal electrodes to the reaction should be eliminated by

insulating the metal electrodes from CO_2 plasma (as shown in Fig. 1b). In this study, the DBD plasma reactor (as shown in Fig. 1b) was used for the following experiments unless otherwise stated. The effect of the property and that of the size of packing beads on CO_2 decomposition were studied by applying $BaTiO_3$ balls (permittivity: 1000; 3 mm in diameter) and glass beads (permittivity: 4.7; 3 mm, 4 mm, and 5 mm in diameter) in the DBD plasma reactor, respectively.

Fig. 2 shows the conversion of CO_2 over those glass and $BaTiO_3$ balls as a function of plasma power. It is apparent that an increase in plasma power resulted in an increase in CO_2 conversion over these packing beads. The CO_2 conversion over these packing beads is in the order of Glass balls (5 mm) ≈ $BaTiO_3$ balls (3 mm) > Glass balls (4 mm) > glass balls (3 mm).

The plasma assisted CO_2 decomposition ran in a stable way in the time range (up to 5 h) tested. Apparent decrease in CO_2 conversion was not observed. The reaction products were CO and O_2. O_3 was not detected in the experiment. No carbon deposition was observed on the glass and $BaTiO_3$ balls after each experiment in the reactor. It is important to mention that the CO/O_2 (molar ratio) is in the range of 1.98-2.02 after reaction, which is in agreement with the stoichiometry of CO_2 decomposition to CO and O_2. Therefore, the further decomposition of CO to C and O_2 was strongly suppressed in a DBD plasma reactor packed with different packing materials.

When the CO_2 conversion over glass balls (3 mm in diameter) and that over $BaTiO_3$ beads (3 mm in diameter) are compared, it is clear that the $BaTiO_3$ balls significantly enhanced the CO_2 conversion by a factor of 9.1-3.1 depending on plasma power dissipated into the reactor.

As shown in Fig. 2, an increase in the diameter of the packing glass balls resulted in a significant increase in CO_2 decomposition. When the diameter of the glass balls was increased from 3 to 5 mm, the conversion of CO_2 increased by a factor of 9.1 at the plasma power of 46W. It is important to note that there was no apparent difference between the CO_2 conversion over glass balls (5 mm in diameter) and that over $BaTiO_3$ balls (3 mm in diameter), which was different from what we expected, and it could not be explained by the permittivity difference of these materials. Therefore, not only the permittivity but also the size of the packing materials played a key role in the CO_2 dissociation in a packed bed DBD plasma reactor.

The mean electron energy in a DBD can be influenced by varying the product of discharge gap d and the gas density n (which is proportional to gas pressure). [37] In the DBD reactor without packing beads, the discharge gap width was 7.5 mm which was large compared to the conventional DBD for O_3 production. A large discharge gap width can lead to the formation of spark-like discharge and lower mean electron energy in a DBD plasma. [37, 38] When the glass beads or $BaTiO_3$ balls are filled into the plasma reactor, the shorter distance near the contacting point between the packing balls can lead to an enhanced local electric field. Furthermore, the maximum electric field strength near the contact points can be significantly higher than that in the void among those packing balls. It has been reported that those balls can refract the electric field, making the local electric field non-uniform and stronger than the

externally applied field by a factor of 10 to 250 depending on the shape, porosity, and permittivity of the beads. [20] Increased electric field strength and higher mean electron energy can be expected in the DBD reactor packed with those balls. In addition to the discharge gap, the dielectric constant of packing materials is a key factor affecting the properties of a DBD plasma. An increase in dielectric constant of those packing beads can result in a further increase in electric field strength near the contacting points between the packing beads and an enhancement in the mean electron energy in the plasma. As a result, the permittivity of the packing beads can affect the mean electron energy in a DBD plasma. [39, 40] It is known that the mean electron energy is an important factor affecting the activation of molecules (excitation, dissociation, or ionization) in a DBD. [40] Recently, computational study demonstrated that the splitting of CO_2 is dominated by electron impact reactions, and predominately by electron impact dissociation in a DBD plasma. [30] Therefore, high dielectric constant materials (for example: $BaTiO_3$) which can generate stronger electric field and higher average electron energy are desirable for efficient dissociation of more stable molecules, such as CO_2 in a DBD plasma.

In addition to the influence of dielectric constant on various reactions, the shape of the $BaTiO_3$ pellets influenced the reaction performance and the discharge characteristics significantly in the reactor with 2 metal electrodes exposed to plasma. [41] The variation of the permittivity of those $BaTiO_3$ pellets (permittivity: 600, 5000, and 10000, respectively) was not a function of the destruction rate of C_6F_6. However, Ogata and co-workers studied the influence of dielectric constant of packing materials on benzene decomposition by applying ferroelectric balls (2 mm in diameter) with different permittivity (20-15000) in a plasma reactor with 2 electrodes exposed to the plasma activated species. It was observed that increasing the dielectric constant of packing materials resulted in higher benzene conversion.

[42] Li and co-workers found that the CO_2 conversion over higher permittivity $Ca_{0.8}Si_{0.3}TiO_3$ is much higher than that over lower dielectric constant Al_2O_3 and SiO_2 glass barriers in a planner DBD reactor with one electrode exposed to plasma. [34] Mei and co-workers reported that the enhancement of mean electron energy and the photocatalytic effect of $BaTiO_3$ balls (1 mm in diameter) in a plasma can enhance the CO_2 conversion in a DBD reactor with one electrode exposed to plasma. [35] It is important to note that above results were based on packed bed plasma reactors with one or two metal electrodes directly contacted with the plasma activated species. [35, 41, 42] When we discuss the effect of packing materials on those reactions, the catalytic effect of metal electrode/electrodes on various reactions can not be ruled out. Yu and co-workers demonstrated that the permittivity and morphology of packing pellets (size: 0.42-0.84 mm) played key roles in CO_2 decomposition in a DBD plasma with 2 metal electrodes insulated by corundum tubes. [36] However, the effect of the pellet size variation on the reaction was not taken into account. By eliminating the influence of the size, the shape of the packing materials and the metal electrode/electrodes, the present study demonstrated that the property of the packing beads influenced the CO_2 decomposition significantly in a DBD plasma. In this study, because the permittivity of $BaTiO_3$ balls (3 mm in diameter) is much higher than that of glass balls with the same size, the mean electric field strength and the average electron energy could be higher in the reactor packed with $BaTiO_3$ balls than that packed with glass balls. Therefore, a higher fraction of the electrons in the plasma could have sufficient energy to activate CO_2 molecules in the reactor packed with $BaTiO_3$ beads, which could result in an enhanced CO_2 conversion. In addition to the difference in permittivity, $BaTiO_3$ and glass balls have different physical and/or chemical properties which might affect CO_2 decomposition in a DBD plasma as well.

As depicted in Fig. 2, in addition to the permittivity, the packing material size is another key factor influencing the reaction in a plasma reactor. Due to their identical permittivity and chemical properties, the difference of the performance of those glass beads in CO_2 dissociation could be attributed to the effect of the variation of discharge properties. In a packed-bed DBD, the micro-discharges mainly take place near the contact points between packing beads and beads/quartz tubes where electric field strength are significantly increased. [43] Although the number of those contact points/micro-discharges was reduced by increasing the size of glass balls, the amount of charge transferred by an individual micro-discharge could be increased at a constant plasma power. In a DBD plasma, higher average energy dissipated in an individual micro-discharge could be achieved with larger glass beads. Therefore, increasing the size of glass balls could lead to higher CO_2 conversion in the DBD plasma.

Meanwhile, one may argue that the total void volume between the packed beads can be increased when glass balls with larger size are packed in the reactor, which may increase the residence time of CO_2 in the DBD plasma, and might be the reason for the increased CO_2 conversion. In this study, the void volume of the DBD plasma reactor packed with 3 mm and 5 mm diameter glass balls was 35 and 39 cm^3, which gives a residence time of CO_2 of 42 and 46.8 seconds, respectively. When the flow rate of CO_2 was decreased from 50 to 44.9 ml/min in the plasma reactor packed with 3 mm glass balls, the residence time of CO_2 was increased from 42 to 46.8 seconds. At the same residence time of 46.8 seconds, the CO_2 conversion over 3 mm glass balls was 1.2, 2.2, 3.7 and 6.4% at the plasma power of 46, 66, 86 and 106W, respectively, which is significantly lower than that over 5 mm glass balls at the corresponding plasma power depicted in Fig. 2. Therefore, the variation of residence time of CO_2 is not the

main reason for the significant difference in CO_2 conversion over those 3 mm and 5 mm glass balls.

The present study reveals that both the permittivity and the size of packing materials affect plasma assisted CO_2 decomposition in a DBD reactor. The size of packing materials could influence a reaction performance in NTPs. Ogata and co-workers studied the influence of the size of $BaTiO_3$ balls (1, 2, and 3 mm in diameter) on benzene abatement in an NTP reactor. [42] The benzene conversion over 1 mm and 2 mm pellets was quite close and higher than that over 3 mm pellets when the SIE was higher than 54kJ/l. In contrast, the benzene conversion over these balls was in the sequence of 3 mm > 2 mm > 1 mm when the SIE was lower than 18kJ/l. Schmidt-Szalowski reported that a DBD reactor packed with large quartz glass grains could enhance ozone generation and energy efficiency.[44] Our previous research work demonstrated that CO_2 and CH_4 conversions over large $BaTiO_3$ beads (3 mm in diameter) are high than that over small $BaTiO_3$ balls (1 mm in diameter) in a DBD plasma reactor.[45] Therefore, the mean energy dissipated in an individual micro-discharge and the number of micro-discharges are important factors affecting a reaction performance in a DBD plasma. Some reactions could be sensitive to the mean energy dissipated in an individual micro-discharge. When the mean energy of an individual micro-discharge is higher than a certain level, an increase in the number of micro-discharges could promote the reaction. It is possible to improve the reaction performance, such as conversion and product selectivity, by optimizing the packing materials in a DBD reactor.

In addition to the dielectric constant and the ball size, the surface area, pore size and pore volume of the packing materials may influence the plasma behaviour and the reaction

performance under plasma conditions.[20, 39, 46] Meanwhile, DBD may initiate photocatalytic chemical process over $BaTiO_3$ beads and other conventional photo-catalyst such as TiO_2.[35, 47, 48] Moreover, the physical and chemical properties of packing materials may affect plasma assisted chemical reactions in a DBD reactor.

3.2 Influence of reactor configuration

The influence of reactor configuration on CO_2 dissociation to CO and O_2 by applying $BaTiO_3$ balls (3 mm in diameter) and glass beads (3 mm in diameter) as packing materials in a DBD reactor was investigated, respectively. The diameter of $BaTiO_3$ beads and that of glass balls is 3 mm unless otherwise stated in the following experiments.

In this study, the effect of exposing a stainless steel mesh to a DBD plasma on CO_2 decomposition was explored: (1) fix the second electrode on the inner surface of the external tube (Fig. 1c); and (2) fix an additional stainless steel mesh (the same size as the stainless steel mesh electrode) on the inner surface of the external tube of the DBD reactor (Fig. 1d). As depicted in Fig. 3, compared with the performance of the corresponding plasma reactor (Fig. 1b), a significant increase in CO_2 conversion by a factor of 5-2.4 (for glass beads) and 1.6-1.4 (for $BaTiO_3$ balls) was observed when the stainless steel mesh electrode was exposed to plasma activated species or when an additional stainless steel mesh was fixed on the inner surface of the external tube of the DBD plasma reactor. Those experimental results also demonstrated that exposing one electrode to the plasma or fixing an additional stainless steel mesh in the DBD reactor does not result in apparent difference in CO_2 conversion. Further

experimental results revealed that there was no obvious CO_2 conversion in the reactor at the wall temperatures (100-140ºC) when plasma was switched off in the experiment.

The insertion of a stainless steel mesh into the DBD reactor either as an electrode or as a metal layer may affect the electrical characteristics, such as discharge capacitance and the breakdown voltage, of the plasma reactor, [49, 50] which could contribute to the enhancement of CO_2 conversion. Meanwhile, the contribution of plasma catalysis resulted from the combination of a stainless steel mesh and plasma activated species can not be ruled out.

CO_2 can be activated on transition metal catalysts. Modelling study reveals that CO_2 can be adsorbed and activated on transition metal surfaces.[51] In this study, in addition to the gas phase CO_2 decomposition by plasma, the decomposition of CO_2 molecules on the surface of stainless steel mesh could be promoted by plasmas at low temperatures. Due to the activation of CO_2 on the electrode, the electrons with lower energy may become effective for CO_2 dissociation on the the electrode. On the other hand, in addition to the homogeneous gas phase reactions of CO and O radicals, when a stainless steel mesh was exposed to the CO and O radicals generated by an NTP, some of the CO and O radicals coud be adsorbed on the stainless steel mesh. The recombination of adsorbed O radicals could form O_2 and the combination of adsorbed O and adsorbed CO could form CO_2 on the mesh at low temperatures and ambient pressure. According to Fig. 3, it was reasonable to suggest that the recombination of O radicals may prevail over the combination of CO with O radicals on the mesh in the discharge.

When a stainless steel mesh is exposed in plasma, apparent improvements in conversion and product selectivity have been observed. It was reported that the electrode materials influenced

CO_2 decomposition apparently in a gas mixture of CO_2 and He in a glow discharge plasma.[52] The CO_2 conversion is in the order of Cu > Au > Rh >Fe ≈ Pd ≈ Pt. Brock and co-workers demonstrated that the metals coated on a fan type plasma reactor can catalyse CO_2 decomposition in a mixture of CO_2 and He at low temperatures and atmospheric pressure.[53, 54] The reactivity of the metal coatings is in the sequence of Rh > Pt ≈ Cu > Pd > Au/Rh ≈ Rh/Au ≈ Au. In a plasma assisted CO_2 and CH_4 conversion to synthesis gas (CO +H_2) and higher hydrocarbons, a stainless steel mesh exposed to the plasma activated species could catalyse the reaction between O radicals and carbon containing intermediates derived from CH_4 for CO in a DBD plasma.[45] These phenomena suggested that when a metal is exposed to the plasma, the property of the metal may influence the adsorption, the activation and hence the reaction performance of chemical reactions in plasma.

In addition to the homogeneous gas phase plasma reactions, a series of heterogeneous reactions may take place on the metal surface under plasma conditions, which can affect the reaction activity and product selectivity. Therefore, when we study the influence of packing materials/solid catalyst on plasma performance and chemical reactions, it is necessary to eliminate the contribution of metal electrode/electrodes to the reaction by insulating those metal electrodes from the plasma activated species. According to the property of a reaction assisted by NTPs, optimizing the metal (or alloy) exposed to the plasma may improve the performance of the reaction in a DBD plasma at low temperatures and ambient pressure.

In this study, the reactor configuration influenced the reaction obviously in a DBD plasma. The insertion of a stainless steel mesh into a plasma reactor may lead to catalytic effect in plasma and/or influence the electrical characteristics of the plasma reactor, which may

contribute to the enhancement of CO_2 conversion at low temperatures and atmospheric pressure.

3.3 Influence of Ni/SiO_2 catalyst

When a catalyst was introduced into the plasma, chemical reactions in a plasma became the combination of gas phase reactions and heterogeneous reactions on the catalyst. Therefore, a catalyst may significantly influence the plasma chemistry of the reaction. The interaction between a DBD and a catalyst is complicated because when the catalyst pellets are packed in a DBD the plasma characteristics could be modified. Meanwhile, the DBD may influence the catalytic properties of the catalyst.

Fig. 4 depicts the influence of plasma power on CO_2 conversion over $BaTiO_3$ balls, and the mixture of a Ni/SiO_2 catalyst and $BaTiO_3$ balls, respectively. Increasing the plasma power results in a substantial increase in CO_2 conversion over a mixture of Ni/SiO_2 and $BaTiO_3$ balls. In comparison to the reaction in the absence of a Ni/SiO_2 catalyst, introducing the catalyst into DBD enhanced the CO_2 conversion by a factor of 1.24-1.31 in the power range tested. When the plasma was switched off, no CO_2 conversion was observed in the reactor packed with a mixture of Ni/SiO_2 catalyst and $BaTiO_3$ balls in the temperature range tested (70-140ºC). Therefore, the enhanced CO_2 decomposition could be attributed to the synergistic effect of NTP and catalysis by the combination of a DBD plasma and a Ni/SiO_2 catalyst.

The mean electron energy (1 – 10 eV) in a DBD plasma is higher than the dissociation energy of CO_2 (5.5eV). In gas phase, the initial step for electron-impact CO_2 dissociation can be described as

$$e + CO_2 \xrightarrow{Plasma} CO + O + e \qquad (4)$$

The O radicals and CO species can be produced directly by electron impact process in plasma (equation 4). The following reactions can influence the final CO_2 conversion and product distribution.

$$O + O + M \xrightarrow{k_1} O_2 + M \qquad (5)$$

$$O + CO + M \xrightarrow{k_2} CO_2 + M \qquad (6)$$

(M reprents the third body of the reaction)

The formed O radicals can either react with other O radicals to form O_2 (equation 5), or react with CO to form CO_2 (equation 6), which can result in a lower CO_2 conversion. The effective rate constant for the 3 body reaction of O + O + M (k_1 = 5.82×10^{-34} cm^6 $molecule^{-2}$ s^{-1}) is 2 order of magnitude larger than the 3 body reaction of O + CO + M (k_2 = 4.44×10^{-36} cm^6 $molecule^{-2}$ s^{-1}) at the reaction temperature of 100 °C.[55] Therefore, the recombination of O radicals prevails over the combination of CO with O radicals in a DBD plasma in gas phase.

A solid catalyst packed in the plasma reactor may reduce the discharge gap width and modify the plasma characteristics by increasing the strength of the electric field, and hence the electron temperature of the energetic electrons in the plasma. Moreover, introducing a catalyst into the plasma changes the homogeneous gas phase chemical reactions into the

combination of gas phase reactions and gas-solid reactions on the catalyst. Therefore, the catalyst property can influence the reaction in NTPs. It has been reported that CO_2 can be adsorbed and activated on a nickel catalyst.[51, 56, 57] The dissociation of CO_2 to adsorbed CO and O can be detected on Ni even at room temperature.[56] A study on CO_2 adsorption and decomposition on Ni by using density functional theory methods reveals that Ni shows favourable thermodynamics and low CO_2 dissociation barriers for CO_2 reduction. The chemisorbed CO_2 is partially negatively charged and has elongated C-O bond lengths and a bent CO_2 structure because of the electron transfer from nickel surface to the antibonding orbital of CO_2.[57] Therefore, the dissociation energy of the chemisorbed CO_2 on the surface of Ni could be lower than that in gas phase (5.5eV). According to the electron energy distribution function (EEDF) in an NTP, some electrons with the energy lower than 5.5eV could be effective for adsorbed CO_2 dissociation on the Ni/SiO_2 catalyst. In comparison with the reaction in the absence of a Ni/SiO_2 catalyst, introducing a Ni/SiO_2 catalyst into the plasma could enhance the electron temperature and decrease the CO_2 bond dissociation energy, which may lead to a synergistic effect of plasma catalysis and result in enhanced CO_2 decomposition.

As shown in Fig. 4, a Ni/SiO_2 catalyst in the plasma can enhance the CO_2 conversion significantly at low temperatures and ambient pressure. A mechanism of CO_2 decomposition over a Ni/SiO_2 catalyst could be proposed based on the experimental results and above discussion (Fig. 5).

Under NTP conditions, in addition to the CO_2 dissociation to CO and O radicals in a gas phase plasma, CO_2 and plasma excited CO_2 molecules can be adsorbed on the surface of a

Ni/SiO_2 catalyst to form adsorbed CO_{2ad}. In an NTP, the energetic electrons can dissociate these CO_{2ad} molecules to form CO_{ad} and adsorbed O_{ad} species on the catalyst. The desorption of CO_{ad} can release CO. At the same time, the recombination of O_{ad}, can form adsorbed oxygen O_{2ad}. The desorption of O_{2ad} can release O_2. Meanwhile, the O_{ad} species may oxidize Ni catalyst to produce NiO on the catalyst, and the NiO could be reduced to Ni by CO_{ad} or CO in the reaction.

It is also possible that the CO and O radicals produced by plasma in gas phase can be adsorbed on the catalyst to form CO_{ad} and O_{ad}. The combination of O_{ad} and CO_{ad} on the Ni catalyst could result in the formation of CO_2. The other reactions, such as the reaction between O_{ad} and CO, and the reaction between O and CO_{ad}, may result in CO_2 formation as well. Various research groups have reported that the recombination of O radicals to O_2 prevails over the combination of CO with O radicals on various solid surfaces at low temperatures.[27, 28, 36, 58]

Temperature is a key factor affecting chemical reactions over catalysts under thermal reaction conditions. To explore the influence of temperature on CO_2 decomposition over a mixture of Ni/SiO_2 catalyst and $BaTiO_3$ balls assisted by a DBD plasma, a tubular furnace was used to keep the plasma reactor wall temperature at 70, 90, 100, 115, 125 and 140° C, respectively.

Fig. 6 shows that the wall temperature of the reactor is an important factor affecting CO_2 decomposition over a mixture of Ni/SiO_2 catalyst and $BaTiO_3$ balls in a DBD plasma. When the reactor wall temperature was lower than 115°C, the variation of reactor wall temperature

does not influence the CO_2 conversion apparently. However, when the reactor wall temperature was increased from 115 to 140ºC, a Ni/SiO_2 catalyst decreased the CO_2 conversion significantly from 23 to 10%. Our further experiment reveals that the variation of wall temperature does not influence the CO_2 conversion obviously in the DBD reactor packed with $BaTiO_3$ balls only in the wall temperature range tested (70-140ºC), indicating that the reverse reaction of CO_2 decomposition over Ni/SiO_2 catalyst became dominant at higher wall temperatures of the reactor.

It was reasonable to suggest that the reactions between CO_{ad} and O_{ad}, CO_{ad} and O, and CO and O_{ad}, over the Ni/SiO_2 catalyst could be promoted at higher wall/reaction temperatures, which could result in lower CO_2 conversion (equation 7-9). Moreover, the NiO can catalyse the oxidation of CO to CO_2 in the reaction.[59, 60]

$$CO_{ad} + O_{ad} \longrightarrow CO_2 \qquad (7)$$

$$CO_{ad} + O \longrightarrow CO_2 \qquad (8)$$

$$CO + O_{ad} \longrightarrow CO_2 \qquad (9)$$

It is important to clarify that the real reaction temperature in the plasma reactor could be higher than the wall temperature of the reactor. Therefore, to achieve a higher CO_2 conversion, it is important to remove the heat produced by plasma to prevent the reverse reaction of CO_2 decomposition over Ni/SiO_2 catalyst in an NTP.

3.4 Catalyst characterization

The fresh and used catalysts after prolonged experiment (5h) at 100ºC were characterized by SEM, BET, XRD and TEM. As shown in Fig. 7, the fresh and spent catalyst samples have hierarchical pore structure. Those SEM images (Fig. 7a and Fig. 7b) revealed that the hierarchical pore structure is stable after the experiment in a DBD plasma. The comparison of the specific surface area between the spent Ni/SiO_2 catalyst (175 m^2/ g) and the fresh one (181m^2/g) demonstrated that the specific surface area of the catalyst does not decrease significantly after the reaction assisted by a DBD plasma.

The XRD patterns of the fresh and spent catalysts were depicted in Fig. 8. The typical peaks corresponding to metallic Ni (44.49°, 51.9° and 76.4°) could be observed in the fresh and spent catalysts. Meanwhile, the peaks corresponding to NiO (37.3°, and 63°) were also detected in the fresh catalyst. The peak corresponding to NiO (43.3°) was quite small in the fresh catalyst and it was overlapped by the strong peak corresponding to metallic Ni (44.49°). After reaction, a shoulder peak (42-47°) corresponding to NiO (43.3°) and metallic Ni (44.49°) was observed in the XRD profile of the spent catalyst, and the intensity of the peaks corresponding to NiO (37.3°, and 63°) increased obviously, indicating that some of the metallic Ni was oxidized to NiO in the reaction at the reactor wall temperature of 100ºC.

As described in 3.1, the conversion of some Ni to NiO on the Ni/SiO_2 catalyst did not result in apparent decrease in CO_2 conversion in a DBD plasma.

According to the TEM images of the Ni/SiO_2 catalyst samples (Fig. 9), the Ni particle size on a Ni/SiO_2 could be decreased to some extent after the plasma assisted CO_2 decomposition. The same result was observed in the NTP assisted CO_2 and CH_4 conversion over a Ni/SiO_2 catalyst at 110 ºC and ambient pressure.[45] Recently, Jwa and co-workers also reported that the size of Ni crystallite decreased after a plasma assisted methanation of CO and CO_2 over Ni/Zeolite catalysts at the reaction temperature of 180-260 ºC and atmospheric pressure. [61]

The metal particle size on a catalyst support is an important factor affecting the activity, selectivity, and stability of the catalyst in a reaction. In thermal catalytic process, high reaction temperatures can lead to agglomeration of Ni particles, which is one of the major drawbacks of the supported nickel catalysts. The catalyst could loss active sites/surface, and consequently be deactivated at higher reaction temperatures due to the sintering of Ni particles.[62-64] In the CO_2 decomposition over a Ni/SiO_2 catalyst promoted by a DBD plasma, it is not the temperature, but the energetic electrons initiating the reaction at low temperatures, which could inhibit the agglomeration of Ni particles on the catalyst. At the same time, the energetic electrons in a strong electric field of DBD plasmas may affect the interaction between Ni particles and SiO_2, which may improve the distribution of Ni particles on the catalyst.

3.5 Energy efficiency

Energy efficiency is a big concern for the implementation of plasma assisted chemical process. The highest possible energy efficiency can be obtained in a microwave plasma because the vibrational levels of CO_2 could be excited selectively, which can promote

efficient CO_2 dissociation in this type of plasma.[22] The calculated energy efficiency of CO_2 dissociation in a microwave plasma could be as high as 23% at reduced pressure of 19.95 torr. However, the energy efficiency of CO_2 conversion is less than 5% in an atmospheric DBD plasma because the electron impact dissociation of CO_2 is the key step in the plasma. [25, 65]

Figure 10 shows the influence of SIE on CO_2 decomposition per unit energy (mmol/kJ) (CPUE) based on the results depicted in Fig. 2, Fig. 3, Fig. 4, and Fig. 6. The permittivity of packing beads, exposing a stainless steel mesh to the plasma, and introducing a Ni/SiO_2 catalyst into the plasma influenced the CO_2 CPUE significantly. The CO_2 CPUE decreases with an increase in SIE over $BaTiO_3$ beads, $BaTiO_3$ beads/mesh, $BaTiO_3$ beads/catalyst, and glass balls (5 mm). In contrast, it increases with an enhancement in SIE over glass beads and glass beads/mesh. It is important to note that replacing glass beads with $BaTiO_3$ balls or glass balls (5 mm) can significantly enhance the CO_2 CPUE by a factor of 9.1 at the SIE of 55.2 kJ/L. Furthermore, exposing a stainless steel mesh electrode to the plasma activated species in a DBD reactor packed with glass balls enhanced the CO_2 CPUE by a factor of 5.1. In comparison with the result packed with glass balls, the combination of $BaTiO_3$ beads with stainless steel mesh significantly enhanced the CO_2 CPUE by a factor of 14.8, and that with a Ni/SiO_2 catalyst increased it by a factor of 11.5.

In this study, the highest energy efficiency (3.4%) of CO_2 decomposition was achieved by exposing a stainless steel mesh to the DBD plasma packed with $BaTiO_3$ balls at CO_2 conversion of 16.3% and SIE of 55.2 kJ/L. Compared with the results in literature[25, 35, 36], it is possible to further enhance the energy efficiency of CO_2 dissociation by optimizing the DBD

reactor configuration, the reaction parameters (such as plasma power, gas flow rate, wall temperature), and introducing a proper catalyst into the plasma.

In a DBD reactor, to increase the mean electron energy and/or reduce the bond dissociation energy of CO_2 molecules by using a catalyst is a key to achieve enhanced CO_2 decomposition and higher energy efficiency. As discussed above, introducing high permittivity packing materials into the discharge gap may enhance the reduced electric field which can result in higher mean electron energy, and then promote the dissociation of CO_2 molecules significantly, and hence enhance the energy efficiency. Furthermore, the bond dissociation energy of CO_2 on transition metal surfaces (such as Fe, Ni) or a Ni/SiO_2 catalyst can be reduced to some extent due to the activation of CO_2 on stainless steel mesh electrode or the Ni/SiO_2 catalyst.[51, 57] Therefore, the energetic electrons with lower energy (< 5.5 eV) may become effective for the adsorbed CO_2 dissociation on stainless steel mesh or the catalyst, which may lead to higher CO_2 conversion and enhanced energy efficiency at low temperatures. However, the Ni/SiO_2 catalyst may catalyse the reverse reaction of CO_2 decomposition at higher reaction temperatures (Fig. 6), which may result in reduced energy efficiency.

In addition to be consumed by the excitation, ionization, and dissociation of molecules, more than 60% of the plasma power converts to heat due to the dielectric heating, the recombination reactions and quenching collisions in a DBD plasma.[66, 67] Substantial fraction of energy supplied to the DBD plasma leads to vibrational excitation of CO_2 molecules. However, the contribution of those vibrationally excited CO_2 molecules to CO_2 dissociation is limited because most of the energy transferred to vibrational excitation of CO_2 converted to

heat in DBD plasmas. [65] Therefore, effective recovering/removing the thermal energy from a DBD plasma reactor can not only prevent the reverse reaction of CO_2 decomposition but also harvest the thermal energy generated by DBD plasmas, which may significantly improve the energy efficiency of plasma assisted CO_2 decomposition at low temperatures and ambient pressure. Furthermore, NTP assisted production of fuels and value-added chemicals from CO_2 using renewable energy sources (solar, wind, nuclear, geothermal, or hydroelectricity) could be a sustainable and potential alternative to reduce CO_2 emission.

Moreover, the utilization of the thermal energy generated by DBD plasmas may lead to energy efficient technologies for plasma assisted conventional catalytic processing. It is known that reactant molecules can be activated on a catalyst at certain temperatures. The energetic electrons generated by an NTP may influence the mechanism of the conventional catalytic reactions at different reaction temperatures. Therefore, the integration of an NTP and conventional thermal catalysis may improve the activity, selectivity, and stability of the catalyst under thermal catalytic reaction conditions with improved energy efficiency. The synergistic effect of plasma catalysis for different chemical process with higher energy efficiency can be achieved by a deep understanding of plasma assisted catalysis at various reaction temperatures and ambient pressure.

4. Conclusions

CO_2 decomposition to CO and O_2 was investigated in a DBD reactor packed with $BaTiO_3$ balls, glass balls with different sizes, and a mixture of a Ni/SiO_2 catalyst and $BaTiO_3$ balls at lower temperatures and ambient pressure. The permittivity and the size of packing beads are

key factors affecting the reaction in an NTP. CO_2 conversion over $BaTiO_3$ beads is higher than that over glass balls because the average electron energy and the mean electric field strength that lead to CO_2 activation/decomposition are higher in a DBD reactor packed with $BaTiO_3$ balls than that packed with glass balls with the same size. Increasing the size of glass balls results in higher CO_2 conversion because the mean energy dissipated in an individual micro-discharge in a DBD plasma packed with larger glass balls was higher than that packed with smaller ones at the same plasma power. The insertion of a stainless steel mesh into a plasma reactor may lead to catalytic effect and/or influence the electrical characteristics of the plasma reactor, which may contribute to the enhancement of CO_2 conversion. In comparison to the reaction in the absence of a Ni/SiO_2 catalyst, introducing a Ni/SiO_2 catalyst to the plasma reactor packed with $BaTiO_3$ balls can promote CO_2 decomposition significantly at low temperatures and ambient pressure because CO_2 could be activated on the Ni/SiO_2 catalyst, which could result in a synergistic effect of plasma catalysis and lead to enhanced CO_2 decomposition. However, the catalyst can catalyse the reverse reaction of CO_2 decomposition at higher wall temperatures (> 115 ºC), which could result in decreased CO_2 conversion and lower energy efficiency. After a prolonged experiment, some metallic Ni was oxidized to NiO and the size of Ni particles had reduced to some extent on the Ni/SiO_2 catalyst. The energy efficiency of plasma assisted CO_2 remediation can be enhanced by increasing the mean electron energy by introducing high permittivity materials such as $BaTiO_3$, optimizing the plasma reactor configuration and packing beads, introducing a proper catalyst, and recovering/removing the thermal energy from the DBD reactor. The integration of NTP assisted direct CO_2 conversion to CO (or synthesis gas ($CO + H_2$) by adding H_2 in the downstream) and the established chemical processing using CO (or synthesis gas) as feedstock may provide an alternative for the production of value-added chemicals and fuels from CO_2.

Acknowledgements

Support of this work by FP7-EU-project COPIRIDE (***Co***mbining ***P***rocess ***I***ntensification-driven Manufacture of Microstructured ***R***eactors and Process Design regarding to ***I***ndustrial ***D***imensions and ***E***nvironment, Grant agreement no.: CP-IP 228853-2), FP7-EU-project PolyCat (Modern **poly**mer-based **cat**alysts and micro-flow conditions as key elements of innovations in fine chemical synthesis, Grant agreement no.: CP-IP 246095-2 is gratefully acknowledged.

References

1. Meinshausen, M.; Meinshausen, N.; Hare, W.; Raper, S. C. B.; Frieler, K.; Knutti, R.; Frame, D. J.; Allen, M. R., Greenhouse-Gas Emission Targets for Limiting Global Warming to 2 Degrees C. *Nature* **2009,** 458, 1158-U96.
2. Matthews, H. D.; Gillett, N. P.; Stott, P. A.; Zickfeld, K., The Proportionality of Global Warming to Cumulative Carbon Emissions. *Nature* **2009,** 459, 829-U3.
3. Wise, M.; Calvin, K.; Thomson, A.; Clarke, L.; Bond-Lamberty, B.; Sands, R.; Smith, S. J.; Janetos, A.; Edmonds, J., Implications of Limiting CO2 Concentrations for Land Use and Energy. *Science* **2009,** 324, 1183-1186.
4. Song, C. S., Global Challenges and Strategies for Control, Conversion and Utilization of CO2 for Sustainable Development Involving Energy, Catalysis, Adsorption and Chemical Processing. *Catal. Today* **2006,** 115, 2-32.
5. Markewitz, P.; Kuckshinrichs, W.; Leitner, W.; Linssen, J.; Zapp, P.; Bongartz, R.; Schreiber, A.; Muller, T. E., Worldwide Innovations in the Development of Carbon Capture Technologies and the Utilization of CO2. *Energy Environ. Sci.* **2012,** 5, 7281-7305.
6. Cuellar-Franca, R. M.; Azapagic, A., Carbon Capture, Storage and Utilisation Technologies: A Critical Analysis and Comparison of Their Life Cycle Environmental Impacts. *J. CO2 Util.* **2015,** 9, 82-102.
7. Centi, G.; Perathoner, S., Opportunities and Prospects in the Chemical Recycling of Carbon Dioxide to Fuels. *Catal. Today* **2009,** 148, 191-205.
8. Omae, I., Recent Developments in Carbon Dioxide Utilization for the Production of Organic Chemicals. *Coord. Chem. Rev.* **2012,** 256, 1384-1405.
9. Li, Y. W.; Chan, S. H.; Sun, Q., Heterogeneous Catalytic Conversion of CO2: a Comprehensive Theoretical Review. *Nanoscale* **2015,** 7, 8663-8683.
10. Wang, W.; Wang, S. P.; Ma, X. B.; Gong, J. L., Recent Advances in Catalytic Hydrogenation of Carbon Dioxide. *Chem. Soc. Rev.* **2011,** 40, 3703-3727.

11. Dimitriou, I.; Garcia-Gutierrez, P.; Elder, R. H.; Cuellar-Franca, R. M.; Azapagic, A.; Allen, R. W. K., Carbon Dioxide Utilisation for Production of Transport Fuels: Process and Economic Analysis. *Energy Environ. Sci.* **2015,** 8, 1775-1789.
12. Saeidi, S.; Amin, N. A. S.; Rahimpour, M. R., Hydrogenation of CO2 to Value-added Products-A Review and Potential Future Developments. *J. CO2 Util.* **2014,** 5, 66-81.
13. Keim, W., Carbon Monoxide-Feedstock for Chemicals, Present and Future. *J. of Organomet. Chem.* **1989,** 372, 15-23.
14. Chen, Z. F.; Concepcion, J. J.; Brennaman, M. K.; Kang, P.; Norris, M. R.; Hoertz, P. G.; Meyer, T. J., Splitting CO2 Into CO And O2 by a Single Catalyst. *Proc. Natl. Acad. of Sci. U. S. A.* **2012,** 109, 15606-15611.
15. Lu, Q.; Rosen, J.; Zhou, Y.; Hutchings, G. S.; Kimmel, Y. C.; Chen, J. G. G.; Jiao, F., A Selective and Efficient Electrocatalyst for Carbon Dioxide Reduction. *Nat. Commun.* **2014,** 5.
16. Wu, H. C.; Chang, Y. C.; Wu, J. H.; Lin, J. H.; Lin, I. K.; Chen, C. S., Methanation of CO2 and Reverse Water Gas Shift Reactions on Ni/SiO2 Catalysts: the Influence of Particle Size on Selectivity and Reaction Pathway. *Catal. Sci. Technol.* **2015,** 5, 4154-4163.
17. Pakhare, D.; Spivey, J., A Review of Dry (CO2) Reforming of Methane over Noble Metal Catalysts. *Chem. Soc. Rev.* **2014,** 43, 7813-7837.
18. Wang, S. B.; Lu, G. Q. M.; Millar, G. J., Carbon dioxide reforming of methane to produce synthesis gas over metal-supported catalysts: State of the art. *Energ. Fuel.* **1996,** 10, (4), 896-904.
19. Eliasson, B.; Egli, W.; Kogelschatz, U., Modelling of Dielectric Barrier Discharge Chemistry. *Pure Appl. Chem.* **1994,** 66, U1766-U1778.
20. Fridman, A., *Plasma Chemistry*. Cambridge University Press: New York, 2008.
21. Kogelschatz, U., Dielectric-Barrier Discharges: Their History, Discharge Physics, and Industrial Applications. *Plasma Chem. Plasma Process.* **2003,** 23, 1-46.
22. Spencer, L. F.; Gallimore, A. D., CO2 Dissociation in an Atmospheric Pressure Plasma/Catalyst System: a Study of Efficiency. *Plasma Sources Sci. Technol.* **2013,** 22, 015019.
23. Vesel, A.; Mozetic, M.; Drenik, A.; Balat-Pichelin, M., Dissociation of CO2 Molecules in Microwave Plasma. *Chem. Phys.* **2011,** 382, 127-131.
24. Heijkers, S.; Snoeckx, R.; Kozak, T.; Silva, T.; Godfroid, T.; Britun, N.; Snyders, R.; Bogaerts, A., CO2 Conversion in a Microwave Plasma Reactor in the Presence of N2: Elucidating the Role of Vibrational Levels. *J. Phys. Chem. C* **2015,** 119, 12815-12828.
25. Kozak, T.; Bogaerts, A., Splitting of CO2 by Vibrational Excitation in Non-Equilibrium Plasmas: a Reaction Kinetics Model. *Plasma Sources Sci. Technol.* **2014,** 23, 045004.
26. Spencer, L. F.; Gallimore, A. D., Efficiency of CO2 Dissociation in a Radio-Frequency Discharge. *Plasma Chem. Plasma Process.* **2011,** 31, 79-89.
27. Mori, S.; Yamamoto, A.; Suzuki, M., Characterization of a Capillary Plasma Reactor for Carbon Dioxide Decomposition. *Plasma Sources Sci. Technol.* **2006,** 15, 609-613.
28. Horvath, G.; Skalny, J. D.; Mason, N. J., FTIR Study of Decomposition of Carbon Dioxide in DC Corona Discharges. *J. Phys. D: Appl. Phys.* **2008,** 41.
29. Paulussen, S.; Verheyde, B.; Tu, X.; De Bie, C.; Martens, T.; Petrovic, D.; Bogaerts, A.; Sels, B., Conversion of Carbon Dioxide to Value-Added Chemicals in Atmospheric Pressure Dielectric Barrier Discharges. *Plasma Sources Sci. Technol.* **2010,** 19, 034015.
30. Aerts, R.; Somers, W.; Bogaerts, A., Carbon Dioxide Splitting in a Dielectric Barrier Discharge Plasma: A Combined Experimental and Computational Study. *Chemsuschem* **2015,** 8, 702-716.
31. Wiegand, W. J.; Nighan, W. L., Plasma Chemistry of CO2-N2-He Discharges. *Appl. Phys. Lett.* **1973,** 22, 583-586.
32. Li, R.; Tang, Q.; Yin, S.; Sato, T., Investigation of Dielectric Barrier Discharge Dependence on Permittivity of Barrier Materials. *Appl. Phys. Lett.* **2007,** 90, 131502.
33. Li, R. X.; Yamaguchi, Y.; Shu, Y.; Qing, T.; Sato, T., Influence of Dielectric Barrier Materials to the Behavior of Dielectric Barrier Discharge Plasma for CO2 Decomposition. *Solid State Ionics* **2004,** 172, 235-238.

34. Li, R. X.; Tang, Q.; Yin, S.; Sato, T., Plasma Catalysis for CO2 Decomposition by Using Different Dielectric Materials. *Fuel Process. Technol.* **2006,** 87, 617-622.
35. Mei, D. H.; Zhu, X. B.; He, Y. L.; Yan, J. D.; Tu, X., Plasma-Assisted Conversion of CO2 in a Dielectric Barrier Discharge Reactor: Understanding the Effect of Packing Materials. *Plasma Sources Sci. Technol.* **2015,** 24, 015011.
36. Yu, Q.; Kong, M.; Liu, T.; Fei, J.; Zheng, X., Characteristics of the Decomposition of CO2 in a Dielectric Packed-Bed Plasma Reactor. *Plasma Chem. Plasma Process.* **2012,** 32, 153-163.
37. Eliasson, B.; Kogelschatz, U., Modeling and Applications of Silent Discharge Plasmas *IEEE Trans. Plasma Sci.* **1991,** 19, 309-323.
38. Kraus, M.; Eliasson, B.; Kogelschatz, U.; Wokaun, A., CO2 Reforming of Methane by the Combination of Dielectric-Barrier Discharges and Catalysis. *Phys. Chem. Chem. Phys.* **2001,** 3, 294-300.
39. Chen, H. L.; Lee, H. M.; Chen, S. H.; Chang, M. B., Review of Packed-Bed Plasma Reactor for Ozone Generation and Air Pollution Control. *Ind. Eng. Chem. Res.* **2008,** 47, 2122-2130.
40. Kogelschatz, U.; Eliasson, B.; Egli, W., Dielectric-Barrier Discharges. Principle and Applications. *J. De Phys. IV* **1997,** 7, 47-66.
41. Takaki, K.; Shimizu, M.; Mukaigawa, S.; Fujiwara, T., Effect of Electrode Shape in Dielectric Barrier Discharge Plasma Reactor for NOx Removal. *IEEE Trans. Plasma Sci.* **2004,** 32, 32-38.
42. Ogata, A.; Shintani, N.; Mizuno, K.; Kushiyama, S.; Yamamoto, T., Decomposition of Benzene using a Nonthermal Plasma Reactor Packed with Ferroelectric Pellets. *IEEE Trans. Ind. Appl.* **1999,** 35, 753-759.
43. Chen, H. L.; Lee, H. M.; Chen, S. H.; Chao, Y.; Chang, M. B., Review of Plasma Catalysis on Hydrocarbon Reforming for Hydrogen Production-Interaction, Integration, and Prospects. *Appl. Catal., B* **2008,** 85, 1-9.
44. Schmidt-Szalowski, K., Catalytic Properties of Silica Packings under Ozone Synthesis Conditions. *Ozone: Sci. Eng.* **1996,** 18, 41-56.
45. Zhang, K.; Mukhriza, T.; Liu, X.; Greco, P. P.; Chiremba, E., A Study on CO2 and CH4 Conversion to Synthesis Gas and Higher Hydrocarbons by the Combination of Catalysts and Dielectric-Barrier Discharges. *Appl. Catal., A* **2015,** 502, 138-149.
46. Yu, Q.; Kong, M.; Liu, T.; Fei, J.; Zheng, X., Non-Thermal Plasma Assisted CO2 Reforming of Propane over Ni/Gamma-Al2O3 Catalyst. *Catal. Commun.* **2011,** 12, 1318-1322.
47. Wallis, A. E.; Whitehead, J. C.; Zhang, K., Plasma-Assisted Catalysis for the Destruction of CFC-12 in Atmospheric Pressure Gas Streams Using TiO2. *Catal. Lett.* **2007,** 113, 29-33.
48. Mei, D. H.; Zhu, X. B.; Wu, C. F.; Ashford, B.; Williams, P. T.; Tu, X., Plasma-Photocatalytic Conversion of CO2 at Low Temperatures: Understanding the Synergistic Effect of Plasma-Catalysis. *Appl. Catal., B* **2016,** 182, 525-532.
49. Wagner, H. E.; Brandenburg, R.; Kozlov, K. V.; Sonnenfeld, A.; Michel, P.; Behnke, J. F., The Barrier Discharge: Basic Properties and Applications to Surface Treatment. *Vacuum* **2003,** 71, 417-436.
50. Falkenstein, Z.; Coogan, J. J., Microdischarge Behaviour in the Silent Discharge of Nitrogen-Oxygen and Water-Air Mixtures. *J. Phys. D:Appl. Phys.* **1997,** 30, 817-825.
51. Liu, C.; Cundari, T. R.; Wilson, A. K., CO2 Reduction on Transition Metal (Fe, Co, Ni, and Cu) Surfaces: In Comparison with Homogeneous Catalysis. *J. Phys. Chem. C* **2012,** 116, 5681-5688.
52. Wang, J. Y.; Xia, G. G.; Huang, A. M.; Suib, S. L.; Hayashi, Y.; Matsumoto, H., CO2 Decomposition Using Glow Discharge Plasmas. *J. Catal.* **1999,** 185, 152-159.
53. Brock, S. L.; Shimojo, T.; Marquez, M.; Marun, C.; Suib, S. L.; Matsumoto, H.; Hayashi, Y., Factors Influencing the Decomposition of CO2 in AC Fan-Type Plasma Reactors: Frequency, Waveform, and Concentration Effects. *J. Catal.* **1999,** 184, 123-133.
54. Brook, S. L.; Marquez, M.; Suib, S. L.; Hayashi, Y.; Matsumoto, H., Plasma Decomposition of CO2 in the Presence of Metal Catalysts. *J. Catal.* **1998,** 180, 225-233.

55. Mallard, W. G.; Westley, F.; Herron, J. T.; Hampson, R. F.; Ferizell, D. H., *NIST Chemical Kinetics Datebase, Windows Version 2Q98 ed.* U. S. Department of Commerce, National Institute of Standards and Technology: Gaithersburg, MD: 1998.
56. Bartos, B.; Freund, H. J.; Kuhlenbeck, H.; Neumann, M.; Lindner, H.; Muller, K., Adsorption and Reaction of CO2 and CO2/O Coadsorption on Ni(110) - Angel Resolved Photoemission (ARUPS) and Electron-Energy Loss (HREELS) Studies. *Surf. Science* **1987,** 179, 59-89.
57. Wang, S. G.; Cao, D. B.; Li, Y. W.; Wang, J. G.; Jiao, H. J., Chemisorption of CO2 on Nickel Surfaces. *J. Phys. Chem. B* **2005,** 109, 18956-18963.
58. Yamamoto, A.; Mori, S.; Suzuki, M., Scale-up or Numbering-up of a Micro Plasma Reactor for the Carbon Dioxide Decomposition. *Thin Solid Films* **2007,** 515, 4296-4300.
59. Conner, W. C.; Bennett, C. O., Carbon Monoxide Oxidation on Nickel Oxide. *J. Catal.* **1976,** 41, 30-39.
60. Wang, D. S.; Xu, R.; Wang, X.; Li, Y. D., NiO nanorings and their unexpected catalytic property for CO oxidation. *Nanotechnology* **2006,** 17, 979-983.
61. Jwa, E.; Lee, S. B.; Lee, H. W.; Mok, Y. S., Plasma-Assisted Catalytic Methanation of CO and CO2 over Ni-Zeolite Catalysts. *Fuel Process. Technol.* **2013,** 108, 89-93.
62. Hashemnejad, S. M.; Parvari, M., Deactivation and Regeneration of Nickel-Based Catalysts for Steam-Methane Reforming. *Chin. J. Catal.* **2011,** 32, 273-279.
63. Bartholomew, C. H.; Sorensen, W. L., Sintering Kinetics of Silica-Supported and Alumina-Supported Nickel in Hydrogen Atmosphere. *J. Catal.* **1983,** 81, 131-141.
64. Wang, S. B.; Lu, G. Q. M., CO2 Reforming of Methane on Ni Catalysts: Effects of the Support Phase and Preparation Technique. *Appl. Catal., B* **1998,** 16, 269-277.
65. Aerts, R.; Martens, T.; Bogaerts, A., Influence of Vibrational States on CO2 Splitting by Dielectric Barrier Discharges. *J. Phys. Chem. C* **2012,** 116, 23257-23273.
66. Kappes, T.; Schiene, W.; Hammer, T., Energy Balance of a Dielectric Barrier Discahreg Reactor for Hydrocarbon Steam Reforming. In *The 8th international symposium on high pressure low temperature plasma chemistry*, Puhajarve, Estonia, 2002; Vol. 2, pp 196-200.
67. Hammer, T., Atmospheric Pressure Plasma Application for Pollution Control in Industrial Processes. *Contrib. Plasma Phys.* **2014,** 54, 187-201.

Figure Captions

Fig. 1 Schematic of the experimental setup and the dielectric-barrier discharge reactor with different configurations: (a) Schematic of the experimental setup; (b) Schematic of the dielectric-barrier discharge reactor one; (c) Schematic of the dielectric-barrier discharge reactor two; (d) Schematic of the dielectric-barrier discharge reactor three; and (e) A picture of the dielectric-barrier discharge reactor one packed with glass balls

Fig. 2 Influence of dielectric barrier materials on CO_2 conversion

(Pressure: 1 bar; Wall temperature: 100 °C; CO_2 Flow rate: 50 mL/min; Frequency: around 20 kHz; 2 electrodes insulated; SIE: 55.2-127.2 kJ/L)

Fig. 3 Influence of reactor configuration on CO_2 conversion

(Pressure: 1 bar; Wall temperature: 100 °C; CO_2 Flow rate: 50 mL/min; Frequency: around 20 kHz; SIE: 55.2-127.2 kJ/L)

(Note: Glass / mesh or $BaTiO_3$ / mesh: a stainless steel mesh electrode was fixed on the internal surface of the external quartz tube of the reactor; Glass + mesh or $BaTiO_3$ + mesh: a stainless steel mesh was fixed on the internal surface of the external quartz tube of the reactor.)

Fig. 4 Influence of Ni/SiO_2 catalyst on CO_2 conversion

(Pressure: 1 bar; Wall temperature: 100 °C; Frequency: around 20 kHz; CO_2 flow rate: 50 mL/min; 2 electrodes insulated; SIE: 55.2-127.2 kJ/L)

Fig. 5 Schematic representation of CO_2 decomposition over a Ni/SiO_2 catalyst assisted by dielectric barrier discharges

Fig. 6 Influence of wall temperature on CO_2 conversion

(Pressure: 1 bar; Wall power: 106 W; Frequency: around 20 kHz; CO_2 flow rate: 50 mL/min; 2 electrodes insulated; SIE: 127.2 kJ/L)

Fig. 7 SEM images of Ni/SiO_2 catalyst samples. (a) Fresh catalyst; (b) Spent catalyst

Fig. 8 XRD patterns of Ni/SiO_2 catalyst samples. (a) Fresh catalyst; (b) Spent catalyst

Fig. 9 TEM images of Ni/SiO_2 catalyst samples. (a) Fresh catalyst; (b) Spent catalyst

Fig. 10 Influence of specific input energy on CO_2 conversion per unit energy

(Pressure: 1 bar; Wall temperature: 100 °C; Frequency: around 20 kHz; CO_2 flow rate: 50 mL/min; power: 46-106 W)

(Note: Glass / mesh or $BaTiO_3$ / mesh: a stainless steel mesh electrode was fixed on the inner surface of the external quartz tube of the reactor)

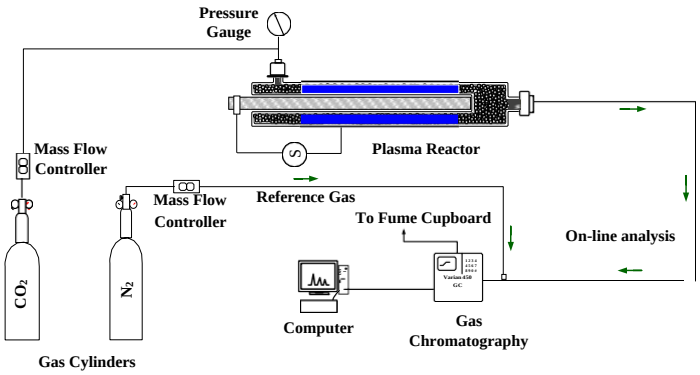

(a) Schematic of the experimental setup

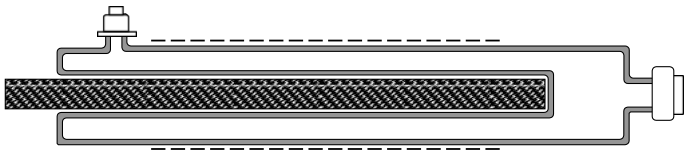

(b) Schematic of the dielectric-barrier discharge reactor one

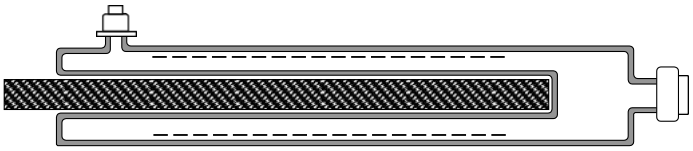

(c) Schematic of the dielectric-barrier discharge reactor two

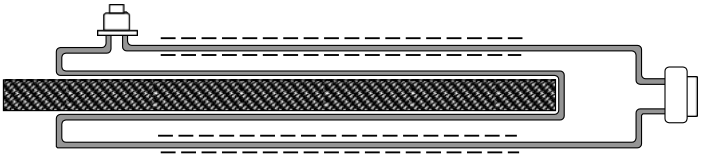

(d) Schematic of the dielectric-barrier discharge reactor three

(e) A picture of the dielectric-barrier discharge reactor one packed with glass balls

Fig. 1 Schematic of the experimental setup and the dielectric-barrier discharge reactor with different configurations: (a) Schematic of the experimental setup; (b) Schematic of the dielectric-barrier discharge reactor one; (c) Schematic of the dielectric-barrier discharge reactor two; (d) Schematic of the dielectric-barrier discharge reactor three; and (e) A picture of the dielectric-barrier discharge reactor one packed with glass balls

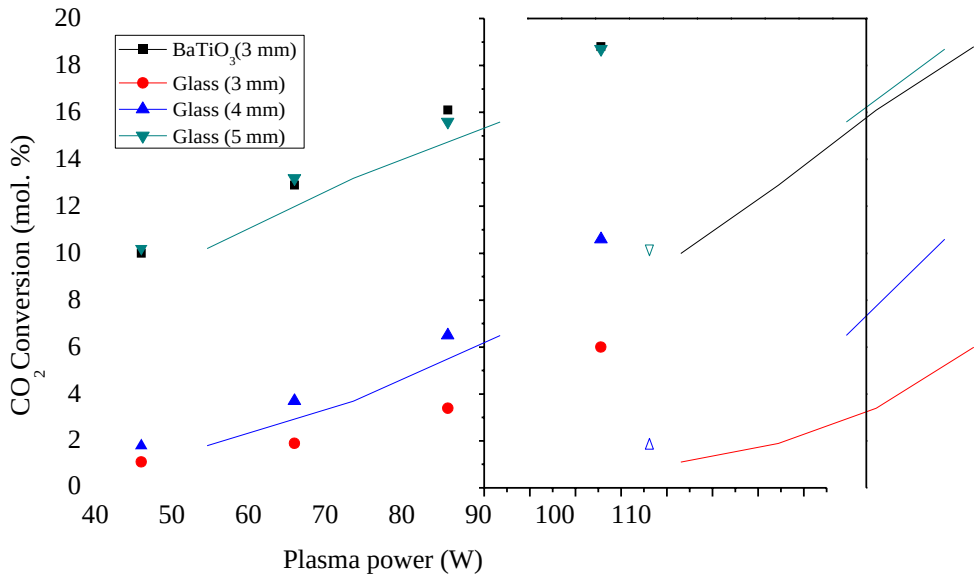

Fig. 2 Influence of dielectric barrier materials on CO_2 conversion

(Pressure: 1 bar; Wall temperature: 100 °C; CO_2 Flow rate: 50 mL/min; Frequency: around 20 kHz; 2 electrodes insulated; SIE: 55.2-127.2 kJ/L)

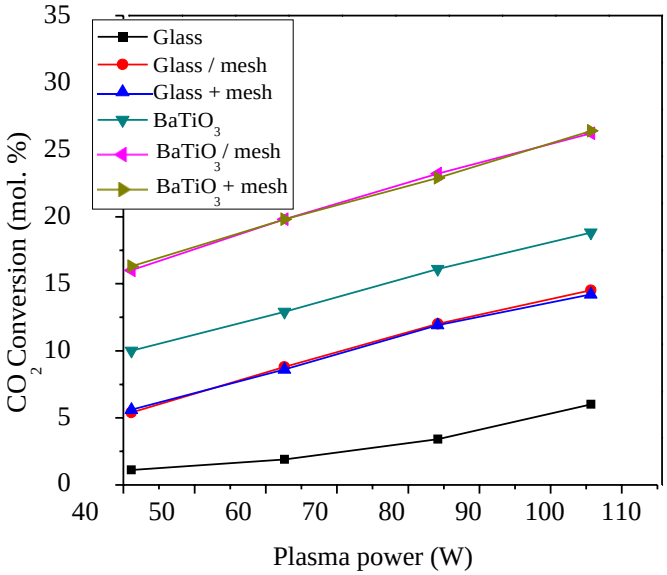

Fig. 3 Influence of reactor configuration on CO_2 conversion

(Pressure: 1 bar; Wall temperature: 100 °C; CO_2 Flow rate: 50 mL/min; Frequency: around 20 kHz; SIE: 55.2-127.2 kJ/L)

(Note: Glass / mesh or $BaTiO_3$ / mesh: a stainless steel mesh electrode was fixed on the inner surface of the external quartz tube of the reactor; Glass + mesh or $BaTiO_3$ + mesh: an additional stainless steel mesh was fixed on the inner surface of the external quartz tube of the reactor.)

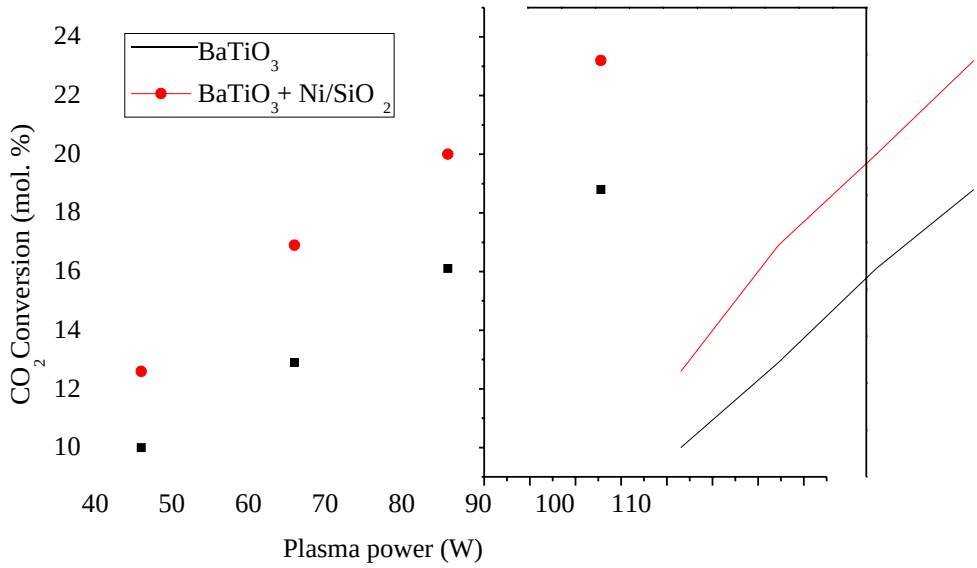

Fig. 4 Influence of a Ni/SiO_2 catalyst on CO_2 conversion

(Pressure: 1 bar; Wall temperature: 100 °C; Frequency: around 20 kHz; CO_2 flow rate: 50 mL/min; 2 electrodes insulated; SIE: 55.2-127.2 kJ/L)

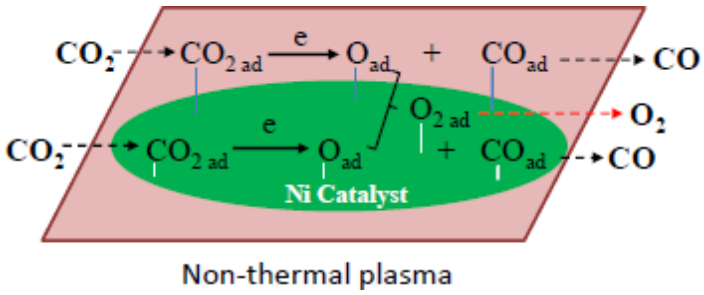

Fig. 5 Schematic representation of CO_2 decomposition over a Ni/SiO_2 catalyst assisted by dielectric barrier discharges

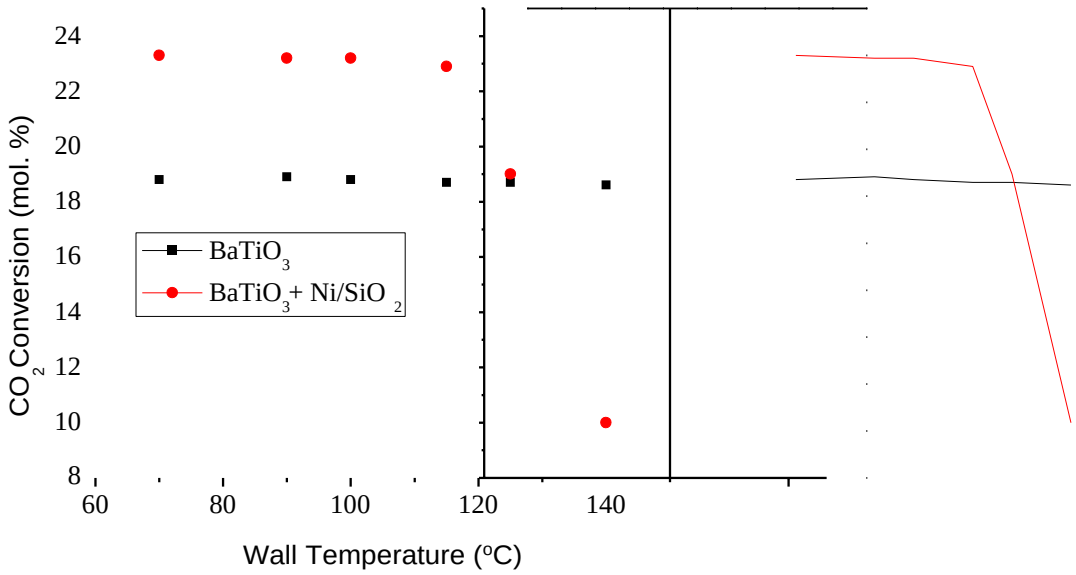

Fig. 6 Influence of wall temperature on CO_2 conversion

(Pressure: 1 bar; Frequency: around 20 kHz; CO_2 flow rate: 50 mL/min; 2 electrodes insulated; SIE: 127.2 kJ/L)

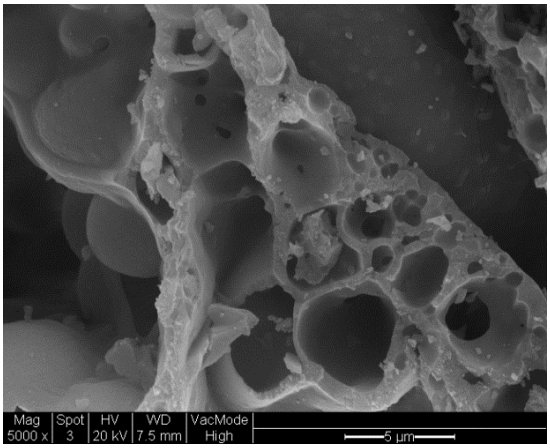

(a)

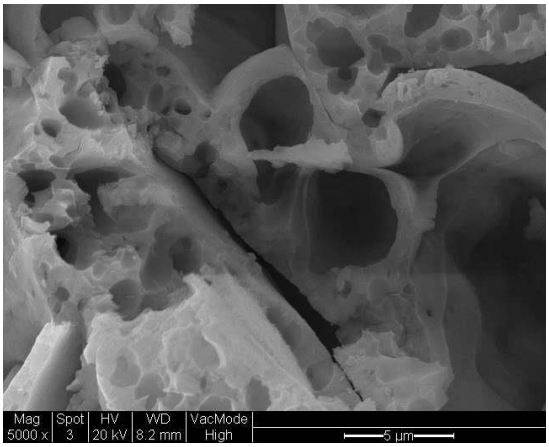

(b)

Fig. 7 SEM images of Ni/SiO_2 catalyst samples. (a) Fresh catalyst; (b) Spent catalyst

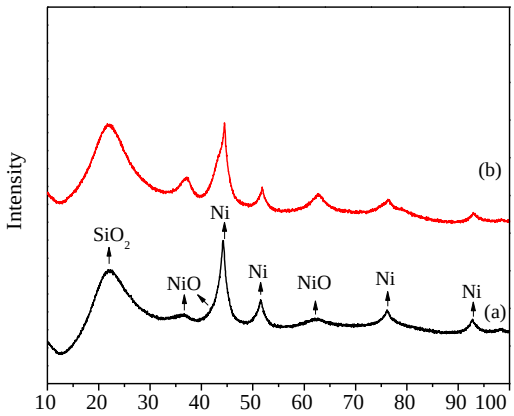

Fig. 8 XRD patterns of Ni/SiO_2 catalyst samples. (a) Fresh catalyst; (b) Spent catalyst

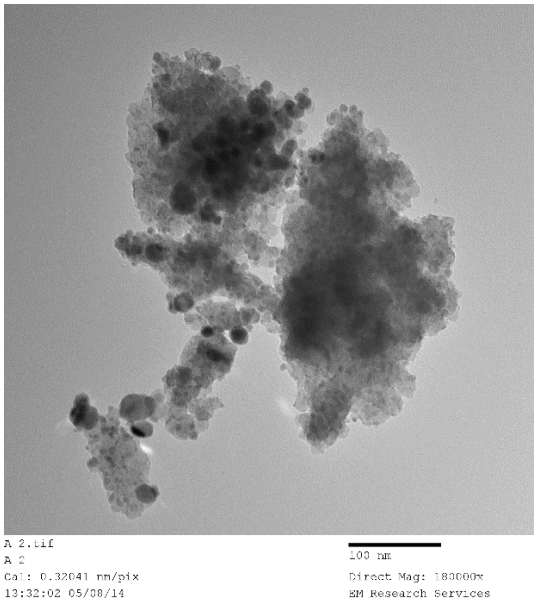

(a)

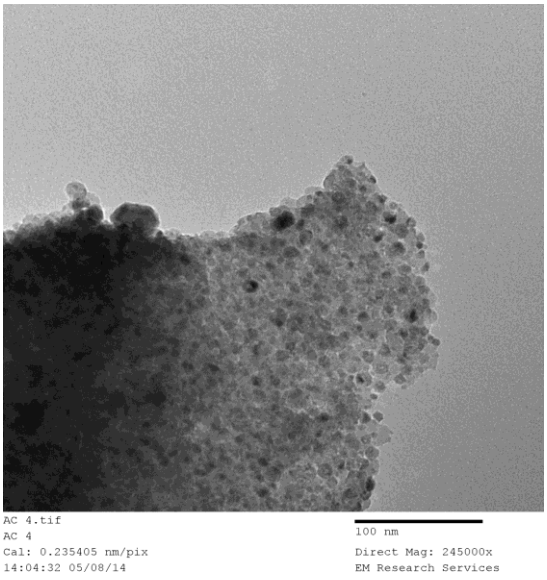

(b)

Fig. 9 TEM images of Ni/SiO_2 catalyst samples. (a) Fresh catalyst; (b) Spent catalyst

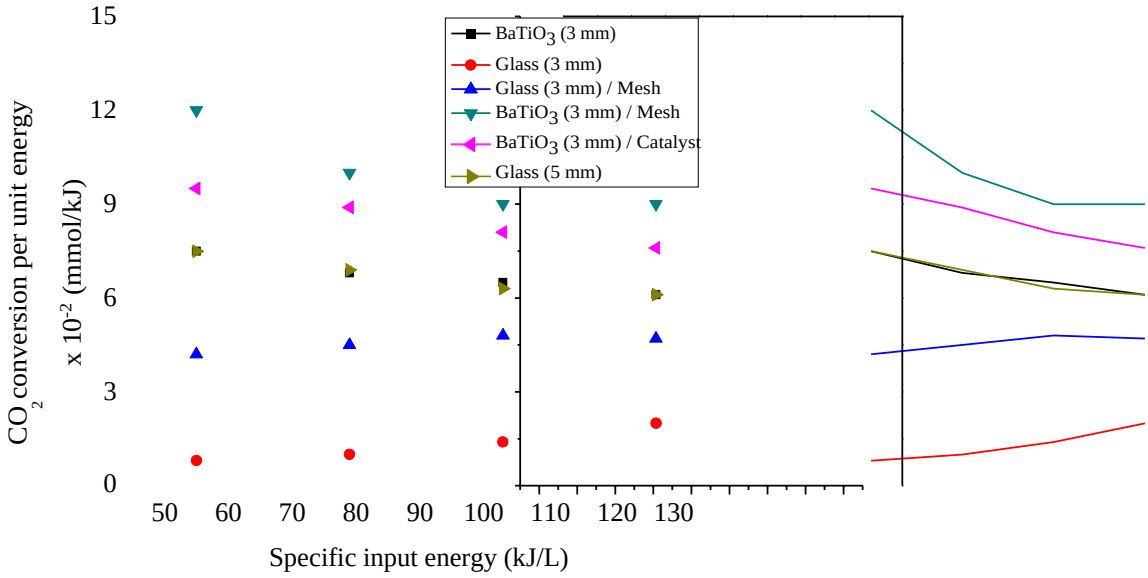

Fig. 10 Influence of specific input energy on CO_2 conversion per unit energy

(Pressure: 1 bar; Wall temperature: 100 °C; Frequency: around 20 kHz; CO_2 flow rate: 50 mL/min; power: 46-106 W)

(Note: Glass / mesh or $BaTiO_3$ / mesh: a stainless steel mesh electrode was fixed on the inner surface of the external quartz tube of the reactor)

TOC

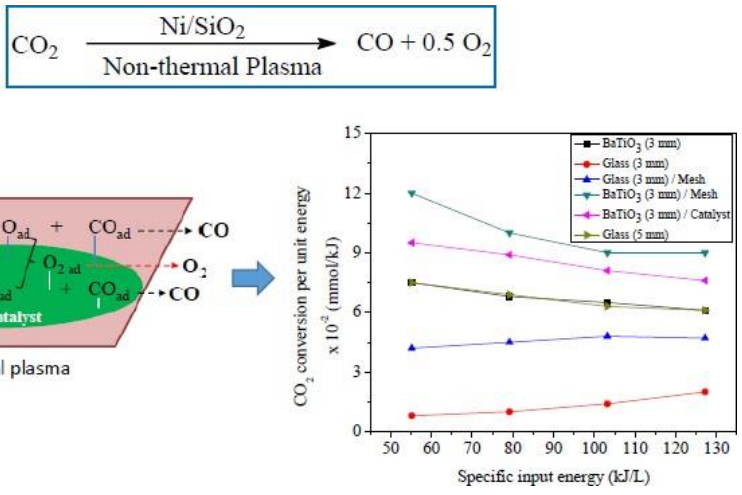
CO2 Ni/SiO2 Non-thermal Plasma CO + 0.5 O2
CO2
CO2 ad
e
Oad
+
COad
CO
O2 ad
O2
Ni Catalyst
Non-thermal plasma
BaTiO3 (3 mm)
Glass (3 mm)
Glass (3 mm) / Mesh
BaTiO3 (3 mm) / Mesh
BaTiO3 (3 mm) / Catalyst
Glass (5 mm)
CO2 conversion per unit energy x 10^2 (mmol/kJ)
Specific input energy (kJ/L)